Modelling Study to Compare the Flow and Heat Transfer Characteristics of Low-Power

Hydrogen, Nitrogen and Argon Arc-Heated Thrusters

Modelling Study to Compare the Flow and Heat Transfer Characteristics of Low-Power Hydrogen, Nitrogen and Argon Arc-Heated Thrusters*

WANG Haixing (王海兴)[1], CHEN Xi (陈熙)[2], PAN Wenxia (潘文霞)[3],
A. B. MURPHY[4], GENG Jinyue (耿金越)[1], JIA Shaoxia (贾少霞)[1]

[1]School of Astronautics, Beijing University of Aeronautics and Astronautics, Beijing 100191, China
[2]Department of Engineering Mechanics, Tsinghua University, Beijing 100084, China
[3]Institute of Mechanics, Chinese Academy of Sciences, Beijing 100190, China
[4]CSIRO Materials Science and Engineering, Lindfield NSW 2070, Australia

Abstract A modelling study is performed to compare the plasma flow and heat transfer characteristics of low-power arc-heated thrusters (arcjets) for three different propellants: hydrogen, nitrogen and argon. The all-speed SIMPLE algorithm is employed to solve the governing equations, which take into account the effects of compressibility, Lorentz force and Joule heating, as well as the temperature- and pressure-dependence of the gas properties. The temperature, velocity and Mach number distributions calculated within the thruster nozzle obtained with different propellant gases are compared for the same thruster structure, dimensions, inlet-gas stagnant pressure and arc currents. The temperature distributions in the solid region of the anode-nozzle wall are also given. It is found that the flow and energy conversion processes in the thruster nozzle show many similar features for all three propellants. For example, the propellant is heated mainly in the near-cathode and constrictor region, with the highest plasma temperature appearing near the cathode tip; the flow transition from the subsonic to supersonic regime occurs within the constrictor region; the highest axial velocity appears inside the nozzle; and most of the input propellant flows towards the thruster exit through the cooler gas region near the anode-nozzle wall. However, since the properties of hydrogen, nitrogen and argon, especially their molecular weights, specific enthalpies and thermal conductivities, are different, there are appreciable differences in arcjet performance. For example, compared to the other two propellants, the hydrogen arcjet thruster shows a higher plasma temperature in the arc region, and higher axial velocity but lower temperature at the thruster exit. Correspondingly, the hydrogen arcjet thruster has the highest specific impulse and arc voltage for the same inlet stagnant pressure and arc current. The predictions of the modelling are compared favourably with available experimental results.

Keywords: low-power arcjet, plasma flow and heat transfer, numerical modelling, propellant-type effects

PACS: 52.80.Mg, 52.65.Kj

1   Introduction

Arc-heated thrusters (or arcjets) have been applied to satellite station-keeping, and have many other potential applications in space propulsion. In the arcjet thruster, gaseous propellant is heated by a DC electric arc to a temperature of about 20 000 K, and the hot gas (plasma) is subsequently expanded through a convergent-divergent nozzle, in which the gas's internal energy is converted into the kinetic energy of an axially-exhausting supersonic jet and thereby generates a thrust force. Since the gaseous propellant in an arcjet thruster can be heated to a much higher temperature, the arcjet thruster may achieve a specific impulse appreciably higher than that of the conventional chemical thruster (e.g., rocket) or the resistance-heated thruster (e.g., resistojet).

Over the past several decades, much efforts have been devoted to the development of arcjet thrusters at different power levels and using a variety of propellants, including argon, hydrogen, nitrogen, a nitrogen-hydrogen mixture simulating decomposed hydrazine, ammonia, etc. Correspondingly, lots of experimental and modelling results have been reported in the literature [1~10] and the references cited therein. However, due to the complexity of physical phenomena involved in the flow and heat transfer processes of the arcjet thrusters, so far our understanding on the energy conversion and thrust force generating processes is still incomplete and thus it is difficult to predict the effect on the thruster per-

formance of changes in power level, propellant type, thruster construction and dimensions, etc.

Recently, experimental systems for studying arcjet thrusters were established at both the Institute of Mechanics, Chinese Academy of Sciences and the School of Astronautics, Beijing University of Aeronautics and Astronautics. A series of experimental studies have been conducted [11,12] on the low-power (kW-class) arcjet thruster characteristics for different operational parameters (arc currents, gas flow rates or inlet gas pressures) and thruster structures, using different working gases (argon, nitrogen, nitrogen-hydrogen mixture, etc.) as the propellants. Concurrently, modelling studies were also performed to understand better the operating characteristics of the low-power arcjet thrusters.

Although many modelling and experimental results concerning hydrogen, nitrogen and argon arcjet thrusters can be found in the literature, and appreciably different thruster characteristics (e.g. different specific impulses, different arc voltages, etc.) are reported, those results are often obtained for different power levels, different thruster structures and/or for different thruster operational parameters. In order to clarify the effect of the propellant type on the thruster characteristics, it is clearly better to compare the thruster characteristics with the same parameters. Hence, in this paper the calculated temperature, axial velocity, Mach number and streamline distributions within the thruster nozzle are compared for an arcjet thruster using hydrogen, nitrogen or argon as the propellant, but for the same thruster structure and dimensions, and for the same inlet-gas stagnant pressure and arc currents.

2 Modelling approach

Fig. 1 is a schematic diagram of the low-power arcjet thruster under study, showing the main dimensions and the domain adopted in calculation.

The main assumptions employed are as follows. **a.** The gas flow in the arcjet nozzle is steady, axisymmetric, laminar and compressible; **b.** The plasma is in the LTE (local thermodynamic equilibrium) state, and thus the thermodynamic and transport properties of hydrogen, nitrogen or argon are completely determined by the local gas temperature and pressure [13~15]; **c.** The plasma is optically thin; **d.** The Lorentz force components are included in both the axial and radial momentum equations, and the Joule heating, radiation loss, viscous dissipation and pressure work are all included in the energy equation; and **e.** the azimuthal (swirling) velocity component is negligible in comparison with the axial velocity component.

Based on these assumptions, the governing equations in a cylindrical coordinate system can be written as follows [15,16].

Mass conservation equation

$$\frac{\partial}{\partial z}\left(\rho u\right) + \frac{1}{r}\frac{\partial}{\partial r}\left(r\rho v\right) = 0. \tag{1}$$

Momentum conservation equations

$$\frac{\partial\left(\rho u u\right)}{\partial z} + \frac{1}{r}\frac{\partial\left(r\rho u v\right)}{\partial r} = -\frac{\partial p}{\partial z} + 2\frac{\partial}{\partial z}\left(\mu\frac{\partial u}{\partial z}\right)$$

$$+\frac{1}{r}\frac{\partial}{\partial r}\left[r\mu\left(\frac{\partial u}{\partial r} + \frac{\partial v}{\partial z}\right)\right] + j_r B_\theta, \tag{2}$$

$$\frac{\partial\left(\rho u v\right)}{\partial z} + \frac{1}{r}\frac{\partial\left(r\rho v v\right)}{\partial r} = -\frac{\partial p}{\partial r} + \frac{2}{r}\frac{\partial}{\partial r}\left(r\mu\frac{\partial v}{\partial r}\right)$$

$$+\frac{\partial}{\partial z}\left[\mu\left(\frac{\partial v}{\partial z} + \frac{\partial u}{\partial r}\right)\right] - 2\mu\frac{v}{r^2} - j_z B_\theta. \tag{3}$$

Energy conservation equation

$$\frac{\partial(\rho u h)}{\partial z} + \frac{1}{r}\frac{\partial(\rho r v h)}{\partial r} = \frac{\partial}{\partial z}\left(\frac{\kappa}{c_p}\frac{\partial h}{\partial z}\right) + \frac{1}{r}\frac{\partial}{\partial r}$$

$$\times\left(r\frac{\kappa}{c_p}\frac{\partial h}{\partial r}\right) + u\frac{\partial p}{\partial z} + v\frac{\partial p}{\partial r} + \Phi + \frac{j_z^2 + j_r^2}{\sigma}$$

$$+\frac{5k_{\mathrm{B}}}{2e}\left(\frac{j_z}{c_p}\frac{\partial h}{\partial z} + \frac{j_r}{c_p}\frac{\partial h}{\partial r}\right) - U_r. \tag{4}$$

Electric potential (current continuity) equation

$$\frac{1}{r}\frac{\partial}{\partial r}\left(r\sigma\frac{\partial\phi}{\partial r}\right) + \frac{\partial}{\partial z}\left(\sigma\frac{\partial\phi}{\partial z}\right) = 0. \tag{5}$$

Here u and v are the axial ($z-$) and radial ($r-$) components of the velocity vector $\mathbf{V}$, p and ϕ are the gas pressure and electric potential respectively, while k_{B} and e are the Boltzmann constant and elementary charge respectively. The physical properties ρ, c_p, h, μ, κ, σ and U_r are the gas density, specific heat at constant pressure, specific enthalpy, viscosity, thermal conductivity, electrical conductivity and radiated power per unit volume of plasma, respectively. These properties are stored in pre-compiled plasma property databases, covering a temperature range of 300 K to 30000 K and a pressure range of 10 Pa to 3×10^5 Pa. The symbol Φ in Eq. (4) denotes the viscous dissipation term, and is calculated using

$$\Phi = \mu\left\{2\left[\left(\frac{\partial v}{\partial r}\right)^2 + \left(\frac{v}{r}\right)^2 + \frac{\partial u}{\partial z}^2\right] + \left(\frac{\partial v}{\partial z} + \frac{\partial u}{\partial r}\right)^2\right.$$

$$\left. -\frac{2}{3}(\nabla\cdot\mathbf{V})^2\right\}. \tag{6}$$

The pressure work and viscous dissipation terms have been included in the energy equation (4) since they are important for the high velocity flow in the thruster nozzle. The current density components j_r and j_z appearing in Eqs. (2)~(4) are calculated using

$$j_r = -\sigma\frac{\partial\phi}{\partial r}, \quad j_z = -\sigma\frac{\partial\phi}{\partial z}; \tag{7}$$

while the self-induced magnetic induction intensity B_θ is calculated using

$$B_\theta = \frac{\mu_0}{r}\int_0^r j_z\xi\mathrm{d}\xi, \tag{8}$$

with μ_0 the permeability in free space.

The LTE assumption is employed here, as in most DC arc modelling studies. However, the LTE assumption leads to a significant underestimate of the values of the gas's electrical conductivity in the near-electrode region, where the electron temperature is appreciably higher than correspondent heavy-particle temperature [15]. It was shown [9,10] that a proper increase in the electrical conductivity in the near-anode region to simulate the non-LTE effects can give reasonable results in modelling studies of arcjet thrusters. RHODES and KEEFER [9] used the following formula to calculate the electrical conductivity σ_n of gas in the near-anode region for a local gas temperature below 10 000 K

$$\sigma_n = (\sigma_{10000} - 10)\, T/10000 + 10 \quad \text{S/m}, \qquad (9)$$

with σ_{10000} the electrical conductivity at 10 000 K for the LTE plasma. In the region with temperatures above 10 000 K, the LTE value is used. Eq. (9) shows that the minimum gas electrical conductivity σ_n in the near-anode region is somewhat larger than 10 S/m. This approach is employed in the present study to allow more realistic treatment of the arc-root attachment at the inner surface of the anode nozzle, but the pressure correction factor suggested in Ref. [9] for the near-wall electrical conductivity was not used since the gas electrical conductivity is not strongly dependent on the gas pressure.

Due to the axisymmetry of the thruster nozzle, only the upper half of the thruster nozzle is taken into account. The calculating domain used in the modelling is denoted as A-B-C-D-E-F-G-H-A in Fig. 1, where A-B-H-A is the cathode, C-D-E-F-J-I-C the anode-nozzle wall, I-J the inner surface of the cylindrical constrictor, J-F the inner surface of the divergent part of the nozzle, B-C the inlet of axially-flowing propellant gas, F-G the thruster exit, and G-H is the nozzle axis. The calculating domain includes the gas flow region within the thruster nozzle and the solid wall region of the anode-nozzle, so the governing equations are used for both the gas and the solid regions and solved in a unified manner. For such a case, one must pay special attention to the solution of the energy Eq. (4), because incorrect results may be obtained if the thermal conductivity and specific heat of solid material are used in the energy equation for the solid wall region, as shown in Refs. [15,17]. This difficulty has been overcome using the following approach. Eq. (4) is solved in the whole calculating domain, with the gas-phase values used for κ, h, c_p, μ and σ in the gaseous region. While solid-phase values of κ and σ are used in the solid region, gas-phase values of h and c_p, at a fixed pressure, are used in the solid region. Using this approach and noting that $h = \int_{T_0}^{T} c_p \mathrm{d}T + h_0$ and thus $\partial h = c_p \partial T$, the energy Eq. (4) in the solid region (with zero-velocity) can be reduced to the following correct form:

$$\frac{\partial}{\partial z}\left(\kappa_s \frac{\partial T}{\partial z}\right) + \frac{1}{r}\frac{\partial}{\partial r}\left(r\kappa_s \frac{\partial T}{\partial r}\right) + \frac{j_z^2 + j_r^2}{\sigma_s}$$

$$+ \frac{5k_B}{2e}\left(j_z \frac{\partial T}{\partial z} + j_r \frac{\partial T}{\partial r}\right) = 0, \qquad (10)$$

where κ_s and σ_s are the thermal conductivity and electrical conductivity of the solid material. The gas specific enthalpy h and specific heat c_p at a fixed pressure are used in the solid region only for expressing the change in local temperature arising from a change in specific enthalpy using $\partial T = \partial h / c_p$, and thus the energy equation in the solid region can be written in the same form as in the gas region.
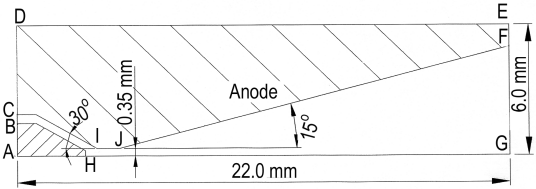

Fig.1 Schematic diagram of the low-power arcjet thruster under study. The dimensions and the calculating domain are also shown

The boundary conditions used in the modelling are as follows. At the gas-inlet section of the arcjet nozzle (i.e. at B-C in Fig. 1), the gas stagnant-pressure is set to be 2.5 atm, the gas temperature is taken to be 500 K, the radial velocity component $v = 0$, and the axial velocity component u is calculated from the given inlet stagnant pressure p_0 and the calculated local static pressure p (obtained by extrapolating the static pressures at the interior grid points neighbouring the inlet boundary) using the compressible flow relation:

$$\left(\frac{p_0}{p}\right)^{(\gamma-1)/\gamma} = 1 + \left(\frac{\gamma-1}{2}\right)\frac{u^2}{\gamma RT}, \qquad (11)$$

where γ is the ratio of specific heats and R is the ideal gas constant. The incoming gas flow rate is determined by the calculation process, as in Ref. [16].

The temperatures at the upstream end of the anode-nozzle wall (C-D) for argon, nitrogen and hydrogen arcjet thrusters are fixed at 1100 K, 1300 K and 1300 K, respectively. These values are in rough agreement with the extrapolated results from the outer-surface temperatures of the arcjet nozzle measured by using an infrared pyrometer at the Institute of Mechanics and at the NASA Lewis Laboratory [18]. On the thruster's outer surfaces D-E and E-F, the local heat flux is governed by thermal radiation to cold surroundings (300 K), and an emissivity of $\varepsilon = 0.3$ is used for tungsten. Along the anode inner-surface C-I-J-F, the heat flux is calculated as the sum of **a.** the heat flux due to convection and conduction, **b.** the enthalpy flux carried by the local electron flux or current density, **c.** the heat flux due to the electron 'condensation' and release of 'condensation heat' [15] at the inner surface of anode, and **d.** the radiation exchange between the plasma and the anode surface.

Zero velocity components are specified at all solid boundaries; axisymmetric conditions are employed

along the nozzle axis; and the temperatures and velocities at the exit section of the thruster are calculated in the iteration process by extrapolating their values at the interior grid points neighbouring the outlet boundary.

Zero current densities are assumed at all the boundaries except for the cathode or anode. The cathode body is included in the calculation domain, and at the rear end of cathode (A-B in Fig. 1) $u = 0$, $v = 0$, $T = 500$ K and $\partial\phi/\partial z = I/(A\sigma_c)$ are used, where I, A and σ_c the arc current, cathode end area and the electrical conductivity of cathode material. $\phi = 0$ is set at the outer surfaces of thruster D-E.

The governing equations are solved using the code developed by HAN and CHEN [16], which is a modified version of the FAST-2D code [19] to include variable gas properties and compressibility. The all-speed SIMPLE algorithm [16], incorporated into the modified FAST- 2D code to simulate the subsonic-supersonic flow, is used to solve Eqs. (1) $\sim$ (5) associated with Eqs. (6) $\sim$ (9) and (11) and the prescribed boundary conditions to obtain the distributions of the velocity, pressure and specific enthalpy (or temperature) in the entire thruster nozzle. A grid mesh of 89 (z-direction) $\times$ 30 (r-direction) are employed in this study. Mass conservation is ensured in the calculation, i.e., the axial gas mass flux is constant for all cross-sections of the nozzle.

For the analysis of the calculated results, typical properties of argon, nitrogen and hydrogen plasmas are listed in Tables 1 and 2 for two characteristic temperatures.

3   Results and discussion

Typical modelling results describing the plasma flow and heat transfer characteristics of the arcjet thrusters using hydrogen, nitrogen and argon as the propellants are presented in Figs. 2 $\sim$ 7, respectively, for a fixed inlet stagnant pressure (2.5 atm) of the propellant. Figs. 2 $\sim$ 5 compare the calculated distributions of tem-

perature, axial velocity, Mach number and streamlines within the thruster nozzle for two different arc currents, 8 A and 10 A.
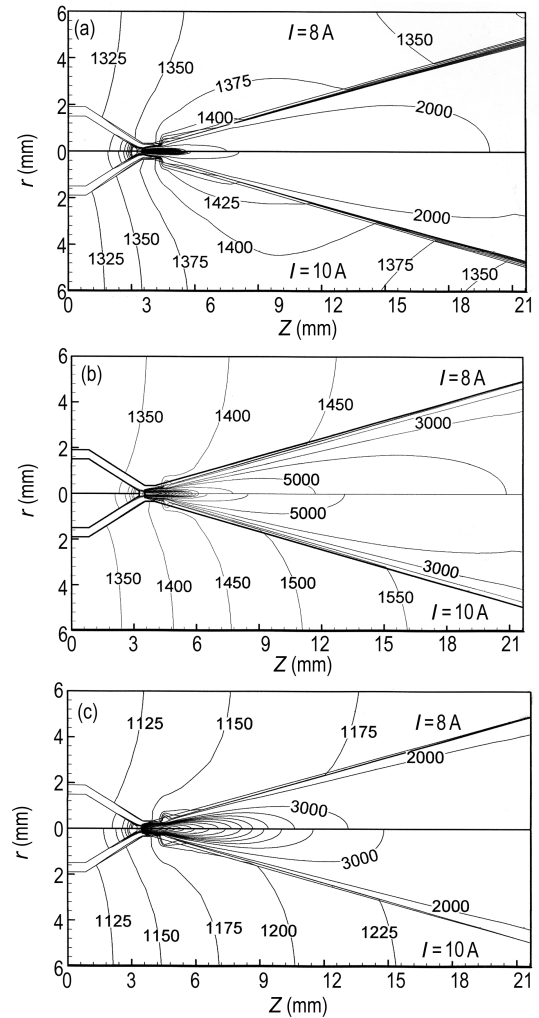

Fig.2   Calculated isotherms within the thruster nozzle for arc currents of 8 A and 10 A with (a) hydrogen, (b) nitrogen and (c) argon as the propellants. Isotherm interval: 1000 K in gas-phase region. Calculated isotherms in the solid wall are also shown

Table 1.   Properties of argon, nitrogen and hydrogen at 15000 K

| Properties | 1.0 atm, 15000 K | | | | | |
	Specific Enthalpy (J/kg)	Specific Heat (J/kg/K)	Electrical Conductivity (S/m)	Thermal Conductivity (W/m/K)	Sonic Velocity (m/s)	Viscosity (kg/m/s)
Ar	3.56×10^7	9.24×10^3	7520	2.36	2430	6.47×10^{-5}
N$_2$	1.28×10^8	2.23×10^4	7468	2.98	4071	5.16×10^{-5}
N$_2$	1.26×10^9	2.79×10^5	6934	6.85	14633	1.92×10^{-5}

Table 2.   Properties of argon, nitrogen and hydrogen at 5000 K

| Properties | 1.0 atm, 5000 K | | | | | |
	Specific Enthalpy (J/kg)	Specific Heat (J/kg)	Electrical Conductivity (S/m)	Thermal Conductivity (W/m/K)	Sonic Velocity (m/s)	Viscosity (kg/m/s)
Ar	2.45×10^6	521	3.018	0.129	1317	1.65×10^{-4}
N$_2$	6.52×10^6	2598	0.356	0.575	1333	1.20×10^{-4}
H$_2$	3.03×10^8	42657	0.710	4.099	7433	5.06×10^{-5}

The isotherms plotted in Fig. 2 show that generally the temperature distributions, and therefore the overall energy conversion processes, in the thruster nozzle are similar. In particular, the gaseous propellant entering the thruster with a temperature of 500 K initially undergoes a rapid temperature rise due to arc heating (Joule heating). The heating of the propellant takes place mainly in the near-cathode and constrictor region where the Joule heating is strong, and the highest plasma temperature occurs near the cathode tip where the current density reaches its maximum. Subsequently, the gas temperature in the divergent part of the nozzle decreases significantly because the thermodynamic expansion dominates the Joule heating. It can be seen that gas temperatures at any given location in the nozzle increase with arc current, as expected. Fig. 2 also shows the temperature distributions in the solid region of the anode-nozzle (tungsten wall). The calculated results indicate that except for the heat loss through radiation from the outer surface D-E, heat conduction towards the upstream end C-D is also an important heat loss mechanism and thus a correct choice of the temperature at the upstream boundary C-D is important for predicting the temperature fields in the solid wall region. It is seen in Fig. 2 that appreciable radial gas-temperature gradients always exist in the thruster nozzle, with an inner hotter core region and an outer cooler edge region. The radial temperature gradient near the inner surface of the nozzle is specifically large in the constrictor region. The gas temperature in the outer cooler gas region decreases along the radial direction and ultimately approaches the temperature on the inner surface of the anode-nozzle wall. This result illustrates the importance of the anode wall temperature in determining the overall performance of the arcjet thruster. Since most of the input propellant flows towards the nozzle exit through the region near the inner surface of the nozzle or in the outer cooler gas region, as is seen in Fig. 5, the temperatures of the inner surface of the anode wall will directly affect the gas temperatures and velocities in the near-wall region, and thus affect the thrust force and specific impulse achieved by the arcjet thruster. In order to increase the calculation accuracy of the nozzle-wall temperatures, the solid region of the anode-nozzle wall was included in the calculating domain in this study to treat the coupling between the heat transfer process in the nozzle flow and that within the solid wall.

The calculated axial velocity and Mach number distributions within the thruster nozzle are shown in Figs. 3 and 4. Because the calculated axial velocity and the corresponding Mach number in the initial convergent segment of the thruster nozzle are small, no isolines of the calculated axial velocity or Mach number can be seen in this segment. Fig. 3 shows that the gaseous propellant flowing into the nozzle is rapidly accelerated to high velocity within a short axial distance; a large radial gradient of the axial velocity exists in the thruster nozzle, and the axial velocity in the thruster
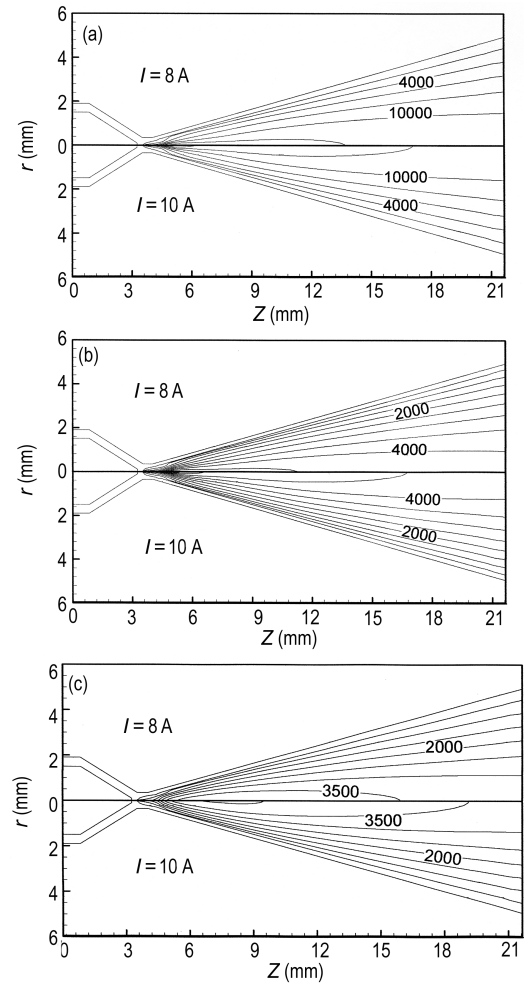

Fig.3 Calculated axial velocity contours within the thruster nozzle for arc currents of 8 A and 10 A with (a) hydrogen, (b) nitrogen and (c) argon as the propellants. Isoline interval: 2000 m/s for hydrogen, and 500 m/s for nitrogen and argon

nozzle increases with arc current. Figs. 3 and 4 show that the flow field in the thruster nozzle can be roughly divided into three distinct regions with different values of the Mach number (Ma), similarly to that in a conventional laval nozzle though the details in flow fields are different. The gas velocities within the convergent segment of the thruster nozzle are relatively low and the corresponding Mach numbers are below 1, i.e. the flow is subsonic. Due to the conversion of both the pressure and thermal energy into the kinetic energy of the gas flow, a transition occurs from the subsonic to the supersonic regime (i.e. a transition from $Ma < 1$ to $Ma > 1$) within the constrictor region. The flow becomes completely supersonic ($Ma < 1$) in the divergent segment of the thruster nozzle. It is worth noting that the predicted axial velocity is always highest near the downstream end of the constrictor, and then decreases gradually along the axis of the divergent nozzle (as also seen in Fig. 6(b)). Such a predicted axial variation of axial velocity is consistent with the measurements [5] for a hydrogen arcjet thruster. This axial variation of axial velocity is different from that for a conventional
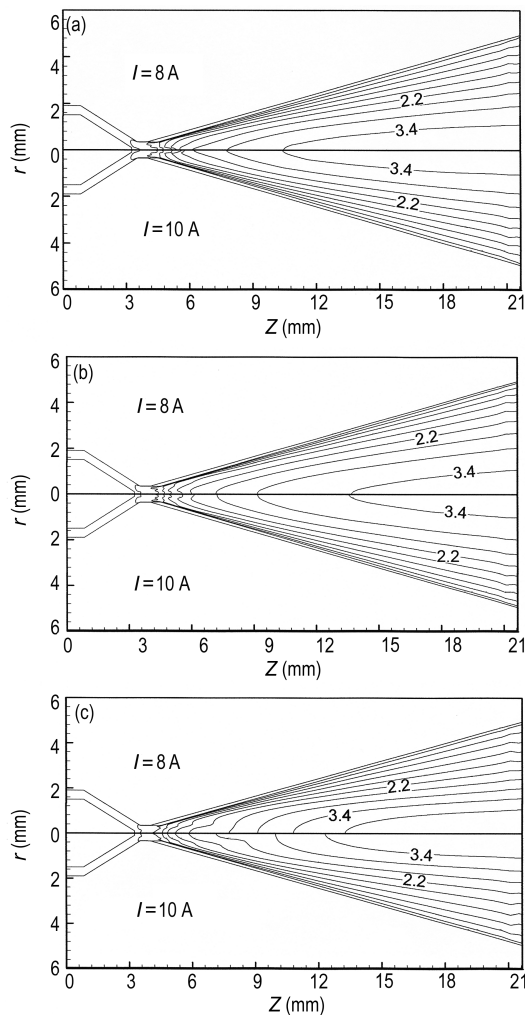
Fig.4 Calculated Mach number contours within the thruster nozzle for arc currents of 8 A and 10 A with (a) hydrogen, (b) nitrogen and (c) argon as the propellants. Isoline interval: 0.4

supersonic divergent nozzle, and represents a new feature of the arcjet nozzle flow, as affected by Joule heating and Lorentz force. Larger axial components of the Lorentz force appearing near the downstream end of the constrictor accelerate the gas flow, and additional Joule heating appearing there also affects the axial velocity. However, as is seen in Fig. 4, the calculated Mach number always increases along the axis of the divergent nozzle, similarly to that in a conventional supersonic divergent nozzle. Due to the appreciable difference in their molecular weights or mass densities, when hydrogen is used as the propellant of the arcjet thruster, the axial velocity, including the exhaust velocity at the nozzle exit, is significantly higher than both of nitrogen arcjet thruster and argon arcjet thruster, as expected. Hence, the specific impulse (corresponding to the average axial velocity at the nozzle exit) of the hydrogen arcjet thruster is significantly higher than that of both the nitrogen arcjet thruster and the argon arcjet thruster. This result is consistent with the available knowledge in the field of electric propulsion [20]. However, Fig. 4 shows that the differences in the calculated distribu-

tions of the Mach number between the hydrogen, nitrogen and argon arcjet thrusters are very small. This is because that the speed of sound also depends on the molecular weight of the gas, and the speed of sound in the hydrogen plasma is appreciably higher than those in both nitrogen and argon plasmas, with a reference in Tables 1 and 2 for values of the speed of sound.

Fig. 5 shows the calculated streamlines within the thruster nozzle. The predicted streamline distributions demonstrate that most of the incoming gaseous propellant flows towards the nozzle exit through the outer cooler region near the anode-nozzle wall. Although a very high temperature core associated with higher gas velocity is produced by the arc in the constrictor region, only a small part of gaseous propellant flows within the arc region. The effect of the central hot arc on the gas flow is likely to generate an electro-thermal "plug", which forces most of the gaseous propellant to flow into the cooler region near the inner surface of the nozzle [21]. This "plug" effect means that the arcjet nozzle flow is different from an ideal one-dimensional nozzle flow, where parameter profiles at successive
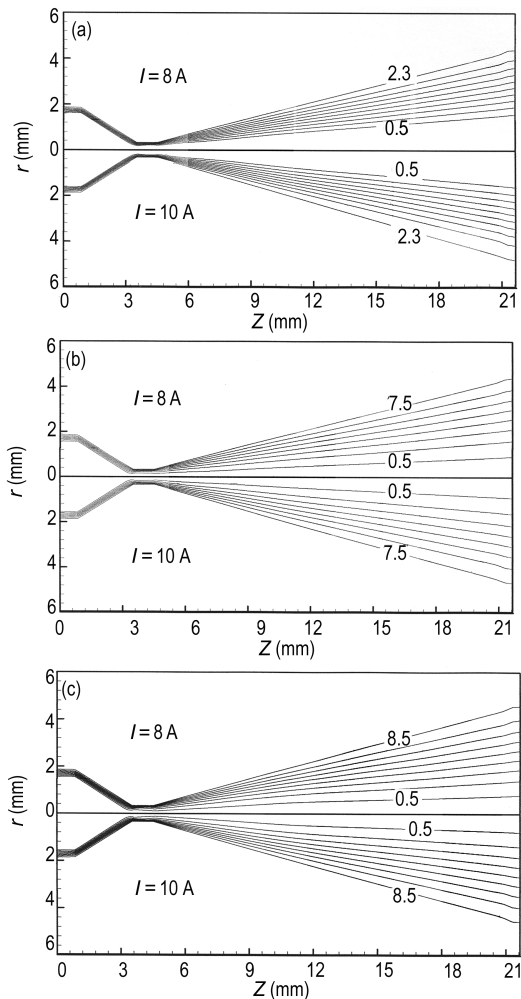

Fig.5 Calculated streamlines within the thruster nozzle for arc currents of 8 A and 10 A with (a) hydrogen, (b) nitrogen and (c) argon as the propellants. Isoline interval: 0.2×10^{-6} kg/s for hydrogen and 1.0×10^{-6} kg/s for nitrogen and argon

cross-sections of the nozzle are uniform, and decreases the effective throat area of the thruster nozzle. Since most propellant flows in the cooler near-wall region, the inner-surface temperatures of the anode-nozzle wall will directly affect the gas temperatures and velocities in the near-wall region and thus affect the thrust force and specific impulse of the arcjet thruster, as discussed above.

The calculated potential distributions within the thruster nozzle are shown in Fig. 6 with an inlet stagnant pressure of 2.5 atm, an arc current of 10 A and using (a) hydrogen, (b) nitrogen and (c) argon as the propellants. It is seen that the potential drop occurs mainly in the near-cathode, near-anode and constrictor region.
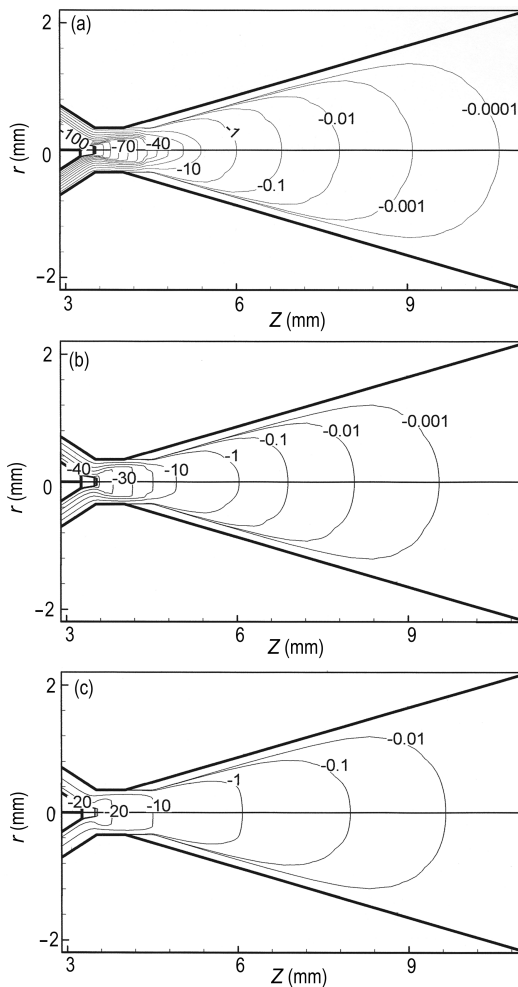

Fig.6 Calculated potential distributions within the thruster nozzle with (a) hydrogen, (b) nitrogen and (c) argon as the propellants with an inlet stagnant pressure of 2.5 atm and an arc current of 10 A

For a fixed inlet-gas stagnant pressure at 2.5 atm and a constant arc current of 10 A, Fig. 7(a) and (b) compare the calculated variations of the plasma temperature and axial velocity along the nozzle axis, respectively, for the hydrogen, nitrogen and argon arcjet thrusters. Fig. 7(a) shows that due to the influences of arc heating and thermodynamic expansion, the plasma
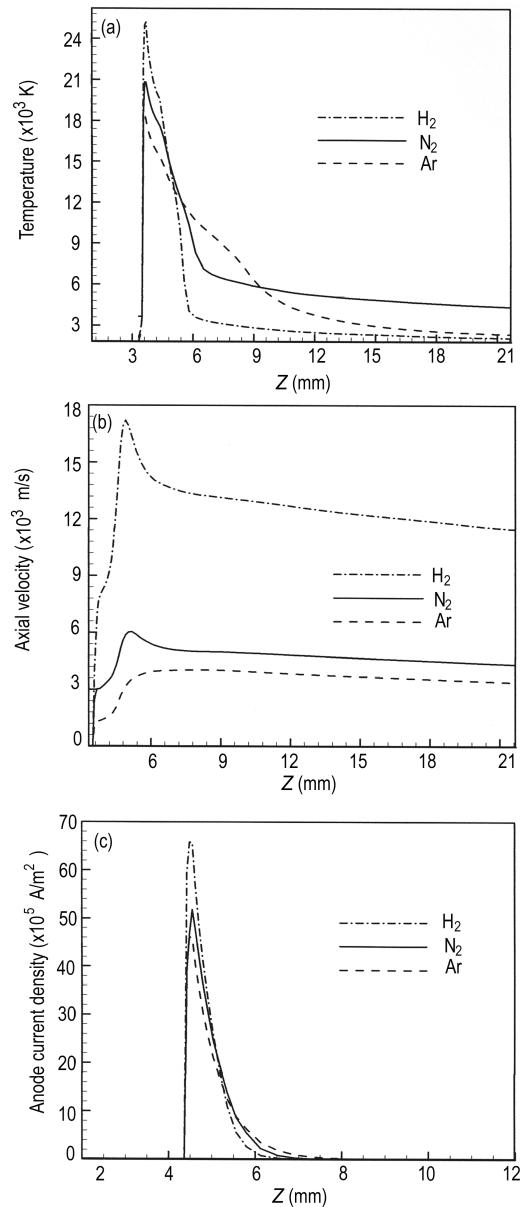

Fig.7 Comparison of calculated variations of (a) plasma temperature and (b) axial velocity along the thruster nozzle axis and (c) current density distributions along the anode surface for an arc current of 10 A, with hydrogen, nitrogen and argon as the propellants

temperature increases very rapidly at first, and then decreases appreciably to comparatively low values as the propellant flows towards the thruster exit. The maximum plasma temperatures appearing in the region near the cathode are 25 210 K, 20 190 K and 18 530 K, respectively, for hydrogen, nitrogen and argon arcjet thrusters. Correspondingly, the highest specific enthalpy in the hydrogen arcjet thruster is significantly higher than that in the nitrogen arcjet thruster and higher again than that in the argon arcjet thruster (cf. Table 1 and Table 2 for the typical values of the specific enthalpy). Hence, much more electric power would be required to supply the hydrogen arcjet thruster than the nitrogen arcjet thruster, for which in turn more power would be required than for the argon arcjet thruster.

Indeed, the arc voltages obtained in this modelling study are 102.2 V, 48.1 V and 24.9 V, respectively, for the hydrogen, nitrogen and argon arcjet thrusters for a constant arc current of 10 A. Due to the high thermal conductivity of hydrogen plasma, the hydrogen arc column is more constricted, i.e. the rate of decrease of temperature is higher than those for either nitrogen or argon as the propellant. The axial velocity distributions along the thruster axis shown in Fig. 7(b) are different from the temperature distributions. The axial velocity increases rapidly at first but then decreases gradually as the propellant flows towards the thruster exit, and the axial velocity assumes its maximum value at the axial location 0.55 mm downstream of the constrictor due to complicated interaction of Joule heating, Lorentz force and thermodynamic expansion. In the divergent part of thruster nozzle, the axial velocities at the nozzle central line decrease from maximum values of 17 200 m/s, 5797 m/s and 4043 m/s to 11 460 m/s, 4308 m/s and 3400 m/s at the thruster exit for the hydrogen, nitrogen and argon arcjet thrusters, respectively. It is also seen in Fig. 7(b) that, due to the different molecular weights of hydrogen, nitrogen and argon, the axial velocities of the hydrogen plasma along the nozzle axis are much higher than those of the nitrogen and argon plasmas. Fig. 7(c) compares the current density distributions calculated along the inner surface of the anode-nozzle for hydrogen, nitrogen and argon arcjet thrusters, and shows that the peak current densities at the anode attachment region are 6.6×10^6 A/m^2, 4.9×10^6 A/m^2 and 4.6×10^6 A/m^2 for the hydrogen, nitrogen and argon arcjet thrusters, respectively. The peak current densities occur at about 0.5 mm downstream of the constrictor. It is also seen in Fig. 7(c) that the arc root attachment at the anode surface for the argon arcjet thruster is more diffusive than those for either nitrogen or hydrogen arcjet thruster. It is worth to note that similar trends in the maximum temperatures and axial velocities were also found in the modelling study of transferred arcs with hydrogen, nitrogen and argon as the working gases [22].

For the case under study, i.e. with the same thruster configuration as well as the same inlet-gas stagnant pressure and arc currents, Fig. 8 compares the calculated radial profiles of the gas temperature (a), axial velocity (b) and Mach number (c) at the nozzle exit plane (F-G in Fig. 1) for the case of a fixed inlet stagnant pressure of 2.5 atm, a constant arc current of 10 A and using hydrogen, nitrogen and argon as the propellants, respectively. As is seen in Fig. 8(a), the predicted temperatures at the centre of thruster exit plane are 2097 K, 4270 K and 2367 K, respectively, for the hydrogen, nitrogen and argon arcjet thrusters, i.e. the nitrogen arcjet thruster assumes the highest exit temperature. An interesting phenomenon observed in Fig. 8(a) is that the highest temperature of argon does not appear at the centre of the thruster exit, i.e. the argon temperature does not decrease monotonically from the central line to the nozzle wall. Such a non-monotonic
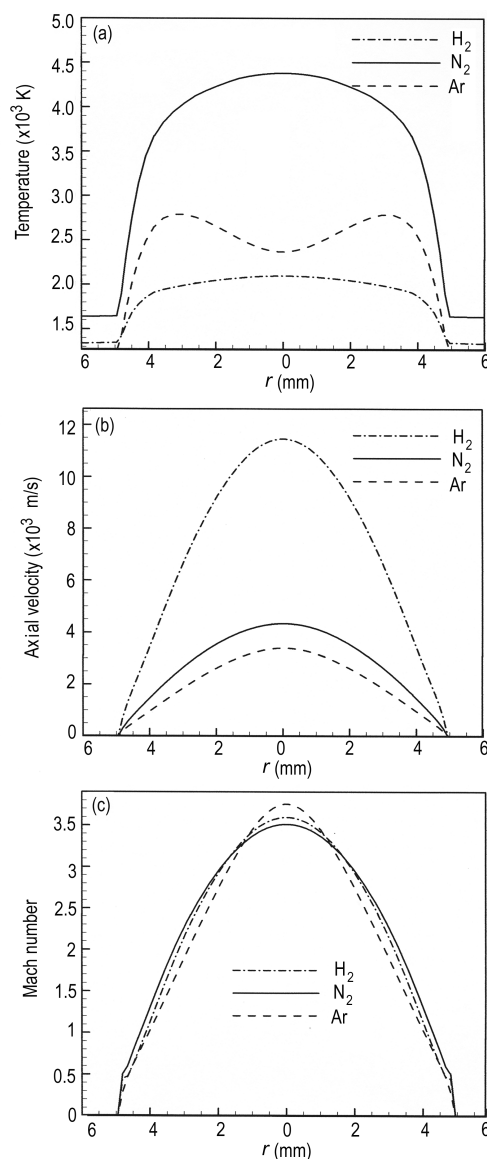

Fig.8 Comparison of calculated radial profiles of (a) plasma temperature, (b) axial velocity, (c) Mach number at the thruster exit plane for an arc current of 10 A, with hydrogen, nitrogen and argon as the propellants

temperature profile differs from available experimental and modelling results for either hydrogen or nitrogen-hydrogen arcjet thrusters [5,23]. However, such a non-monotonic temperature profile was observed by WALKER [24] in an experimental study of a helium arcjet thruster. The non-monotonic temperature profile indicates that the gas in the central region of the nozzle expands to a temperature lower than that in its outer region, while the gas temperatures in that outer region are appreciably higher than the nozzle-wall temperature. Fig. 8(b) and (c) show that the predicted maximum axial velocities at the arcjet exit are 11 460 m/s, 4308 m/s and 3400 m/s, while the highest Mach numbers are 3.59, 3.55 and 3.75, respectively, for the hydrogen, nitrogen and argon arcjet thrusters. Although the magnitudes of the axial velocity at the exit of arcjet thruster for the three propellants are different due to their different molecular weights (with a much larger

exit velocity for the hydrogen arcjet thruster), the Mach number profiles are almost the same because the sonic velocity also depends on the molecular weight of the gases, as mentioned above.

In this study, the inlet axial velocity of the gas is calculated using Eq. (11) from the pre-set stagnant pressure and the local static pressure, rather than from a pre-set gas flow rate. The mass flow rate of the propellant gas is determined by the calculation process itself [16]. After a converged solution was obtained, the calculated gas density ρ and axial velocity u at the nozzle exit section can be used to calculate the mass flow rate G of the propellant gas using $G = \int_0^{r_0} (\rho u) 2\pi r \mathrm{d}r$, while the specific impulse I_{sp} of the arcjet thruster, defined as the thrust force per unit weight flow rate of propellant and with s as its unit, is calculated using $I_{\mathrm{sp}} = F/(Gg) = \int_0^{r_0} (\rho u^2) 2\pi r \mathrm{d}r/(Gg)$. Here r_0 is the radius of the nozzle exit, and F and g are the thrust force and the gravitational acceleration, respectively. For the case with inlet stagnant pressure of 2.5 atm and arc current of 10 A, the calculated mass flow rates are 15.2 mg/s, 48.6 mg/s and 53.3 mg/s, the thrust forces are 111 mN, 133 mN and 113 mN, and the specific impulses are 731 s, 273 s, and 212 s, for hydrogen, nitrogen and argon arcjet thrusters, respectively.

Our modelling results can be compared with the available experimental data. Concerning the kW-class hydrogen arcjet thruster, CAPPELLI and his coworkers [5,25,26] reported the experimental results using an arcjet thruster designed and built at the NASA Lewis Research Center. The thruster nozzle consisted of a 0.635-mm-diameter constrictor, a divergent nozzle with half-angle of 20 degrees, and an exit/constrictor area ratio of 225 [25]. For a mass flow rate of hydrogen propellant of 13.3 mg/s and an input electric power of 0.994 kW, the gas temperature measured by a spectroscopic method near the centre of the nozzle exit was about 2050 K [26]. The axial velocity, measured by using a laser-induced fluorescence method, decreases monotonically along the nozzle axis from the peak value of approximately 17.5 km/s at the axial location 1.3 mm downstream from the constrictor to around 12 km/s at the exit plane [5]. Although accurate comparison of our modelling results with their experimental data is impossible due to the different constrictor diameters (0.70 mm vs. 0.635 mm), exit/constrictor area ratio (200 vs. 225), semi-angle of diverging nozzle segment (15º vs. 20º) and operational parameters of the hydrogen arcjet thrusters employed in our modelling study, reasonable agreement can still be seen. The modelling results corresponding to the measured values (listed above) of 13.3 mg/s, 0.994 kW, 2050 K, and 17.5 km/s at the location 1.3 mm downstream of the constrictor decreasing to around 12 km/s at the nozzle exit, are 15.2 mg/s, 1.022 kW, 2097 K, and 17.2 km/s at the location 0.55 mm downstream of the constrictor decreasing to 11.5 km/s at the nozzle exit, respectively.

Plasma sheaths at the cathode and anode surfaces are not included in the present modelling study. Devi-ations from LTE are only considered in the calculation of the electrical conductivity by empirically enhancing its values in the region near the anode surface, as suggested in Ref.[9]. A more comprehensive modelling approach should include plasma sheaths and more complete treatment of non-LTE effects, but this remains a highly challenging task due to the lack of reliable models and property data. Even the question of how to calculate the gas species composition and the thermodynamic and transport properties of two-temperature plasmas (which are a class of non-LTE plasma) is still being seriously debated in the plasma science and technology community [27].

4 Conclusions

A modelling study was carried out to compare the plasma flow and heat transfer characteristics of low-power hydrogen, nitrogen and argon arcjet thrusters for the same thruster structure and operational parameters (inlet-gas stagnant pressure and arc current). The results show that the common features of the arcjet thrusters using different propellants are as follows. The propellant is heated by Joule heating mainly in the near-cathode and constrictor region, with the highest plasma temperature appearing near the cathode tip; similarly to a conventional laval nozzle flow (although details in flow field details are different), the flow in the arcjet convergent-divergent nozzle can be divided into subsonic, transonic and supersonic flow regimes with the transition from subsonic to supersonic regime occurring within the constrictor region. The highest axial velocity appears inside the divergent nozzle (near the downstream end of the constrictor) instead of at the nozzle exit. Most of the input propellant gas flows towards the thruster exit through the cooler region near the anode-nozzle wall. Due to their appreciably different properties, using hydrogen, nitrogen or argon as the propellant leads to some quite different thruster characteristics. For the same inlet stagnation pressure and arc current, the average axial velocity at the thruster exit (and therefore the specific impulse) for the hydrogen arcjet is significantly higher than that for the nitrogen arcjet and even higher again than that for the argon arcjet, while the maximum temperature at the exit plane for the hydrogen thruster is lower than that for the nitrogen or argon thruster. Although LTE is assumed, with the only non-LTE effect included being an increased gas electrical conductivity in the near-wall region, the modelling predictions are reasonably consistent with the available experimental results for the hydrogen arcjet thruster.

References

1 John R R, Bennett S, Connors J F. 1963, AIAA Journal, 1: 2517

2 Todd J P, Sheets R E. 1965, AIAA Journal, 3: 122

3 Lichon P G, Sankovic J M. 1996, J. Propulsion and Power, 12: 1018

4 Sanchez M M, Miller S A. 1996, J. Propulsion and Power, 12: 1035

5 Cappelli M A and Storm P V. 1996, J. Propulsion and Power, 12: 1070

6 Auweter-Kurtz M, Glocker B, Golz T, et al. 1996, J. Propulsion and Power, 12: 1077

7 Zhang F Y, Fujiwara T, and Komurasaki K. 2001, Applied Optics, 40: 957

8 Glocker B, Auweter-Kurtz M, Goelz T M, et al. 1990, Medium power arcjet thruster experiments. Presented at the 21st Int. Electric Propulsion Conf. (Orlando, USA, 1990). AIAA Paper No. 90-2531, America Institute of Aeronautics and Astronautics, Virginia, USA

9 Rhodes R P, Keefer D. 1990, Numerical modeling of an arcjet thruster. Presented at the 21st Int. Electric Propulsion Conf. (Orlando, USA, 1990) AIAA Paper No. 90-2614, America Institute of Aeronautics and Astronautics, Virginia, USA

10 Butler G W, King D Q. 1992, Single and two-fluid simulations of arcjet performance. Presented at the 28th Joint Propulsion Conf. and Exhibit. (Nashville, USA, 1992) AIAA Paper No. 92-3104, America Institute of Aeronautics and Astronautics, Virginia, USA

11 Pan W X, Li T, Wu C K, et al. 2009, Chin. Phys. Lett., 26: 125201

12 Xin-Ai Zhang, Hai-Bin Tang, Yu Liu, et al. 2009, Effects of propellant type on low power arcjet thruster performance. Presented at the 19th Int. Symp. on Plasma Chemistry (Bochum, Germany, 2009) Paper No. P3.12.5. Ruhr University, Bichum, Germany

13 Murphy A B, Arundell C J. 1994, Plasma Chem. Plasma Process., 14: 451

14 Murphy A B. 2000, Plasma Chem. Plasma Process., 20: 279

15 Chen Xi. 2009, Heat Transfer and Fluid Flow under Thermal Plasma Conditions. Science Press, Beijing (in Chinese)

16 Han P, Chen Xi. 2001, Plasma Chemistry and Plasma Processing, 21: 249

17 Chen Xi, Han P. 2000, Int. J. Heat Fluid Flow, 21: 463

18 Megli T W. 1995, A nonequilibrium plasmadynamics model for nitrogen/hydrogen arcjets. [PhD] Illinos, University of Illinois at Urbana-Champaign, Urbana, USA

19 Zhu J. 1991, FAST-2D: A Computer Program for Numerical Simulation of Two-Dimensional Incompressible Flows with Complex Boundaries. Report No. 690, Institute for Hydromechanics, University of Karlsruhe, Karlsruhe, Germany

20 Jahn R G. 1968, Physics of Electric Propulsion. McGraw-Hill, New York

21 Miller S A. 1994, Multifluid nonequilibrium simulation of arcjet thrusters. [PhD] Massachusetts, Massachusetts Institute of Technology, Boston, USA

22 Murphy A B, Tanaka M, Yamamoto K, et al. 2009, J. Phys. D: Appl. Phys., 42: 194006

23 Bufton S A, Burton R L, Krier H. 1999, J. Propulsion and Power, 15: 735

24 Walker Q E. 2007, Characterization and novel applications of the helium arcjet. [PhD] Stanford Uninversity, Stanford, USA

25 Storm P V, Cappelli M A. 1998, Applied Optics, 37: 486

26 Storm P V, Cappelli M A. 1995, High spectral resolution emission study of a low power hydrogen arcjet plume. Presented at the 26th AIAA Plasmadynamics and Lasers Conference (San Diego, USA, 1995). AIAA Paper No. 95-1960, America Institute of Aeronautics and Astronautics, Virginia, USA

27 Rat V, Murphy A B, Aubreton, et al. 2008, J. Phys. D: Appl. Phys., 41: 183001